

Available online at www.sciencedirect.com

ScienceDirect

Procedia CIRP 58 (2017) 543 – 548



16th CIRP Conference on Modelling of Machining Operations

Microstructure Simulations for Orthogonal Cutting via a Cellular Automaton Model

Ninggang Shen, Avik Samanta, and Hongtao Ding*

Department of Mechanical and Industrial Engineering, University of Iowa, Iowa City, Iowa 52242, USA

* Corresponding author. Tel.: +1-319-335-5674. E-mail address: hongtao-ding@uiowa.edu (H. Ding)

Abstract

In this work, a Cellular Automaton (CA) model is for the first time developed to predict material microstructure evolution during cutting processes. Prior to the CA simulation, the dynamic thermomechanical loadings of work material, Aluminum Alloy 1100, induced by various orthogonal cutting conditions are simulated by finite element-based cutting models. Evolution of dislocation density is modeled using the CA model in MATLAB for the work material subjected to these loading conditions. Multiple mechanisms of microstructure evolution are coupled in the CA model including severe plastic deformation, dynamic recovery, dynamic recrystallization, and thermally-driven grain growth.

© 2017 The Authors. Published by Elsevier B.V. This is an open access article under the CC BY-NC-ND license (http://creativecommons.org/licenses/by-nc-nd/4.0/).

Peer-review under responsibility of the scientific committee of The 16th CIRP Conference on Modelling of Machining Operations

Keywords: Cellular Automaton; Microstructure; Dynamic Recrystallization; Cutting; Severe Plastic Deformation

1. Introduction

Recently, metal material microstructure change through the cutting process has generated a great interest among manufacturing research community [1–4]. During the cutting process, complex dynamic thermomechanical loading condition accompanied with severe plastic deformation (SPD) occurs inside the work material and often induces changes in work material microstructure. For some critical cutting conditions, high cutting process temperatures can reach 80-90% of the melting point (T_m) for the work material, accompanying with a high plastic strain and a high strain rate on the order of $10^4~{\rm s}^{-1}$. Under these elevated temperatures, dynamic recrystallization (DRX) subjected to SPD is considered as a main mechanism for the microstructure evolution [1,3,5].

Modeling and simulations of microstructure evolution is critical to predict the mechanical properties of metal materials after machining. DRX kinetics and thermally-driven grain growth have been developed for various metal materials [6–10]. Finite Element (FE)-based process models are often implemented to model DRX and grain growth of homogenized

work material during hot working processes [11,12]. Cellular Automaton (CA) method has also been applied to simulate the microstructure evolution governed by DRX during the hot forming processes of various metals [13–17].

However, it is still a great challenge to model the microstructure evolution governed by DRX during machining processes due to the highly dynamic thermomechanical loadings. Previous CA models mainly focused on quasi-static loading conditions or conditions with low strain rates. In recent years, phenomenological relationships using Zener–Hollomon and Hall-Petch equations have been applied in FE-based cutting simulations to predict the final grain size distribution [18–23]. However, these methods are unable to capture the intricate dynamic process of recrystallization or grain refinement process.

The dislocation density-based numerical framework developed by the authors has been the first known attempt to model microstructure evolution subjected to SPD during various cutting processes, typically for temperatures well below the initiation temperature of DRX [24–26]. In this framework,

the internal state variables were used to evaluate the dislocation generation due to plastic deformation, dislocation annihilation by dynamic recovery, and interaction between the dislocation cell interiors and cell walls. Recently, dislocation density-based approach have been adapted by more researchers to predict the microstructure evolution in machining [27–31].

In this paper, a two-dimensional (2D) CA model is for the first time developed to model microstructure evolution during orthogonal cutting. Prior to the CA simulation, the dynamic thermomechanical loadings of work material, Aluminum Alloy 1100 (AA 1100), induced by various orthogonal cutting conditions are firstly simulated by a FE-based cutting models. Then, a new model of dislocation density evolution is developed using MATLAB for the work material subjected to these loading conditions. Multiple mechanisms of microstructure evolution are coupled through dislocation density dynamics in the CA model including SPD, dynamic recovery, DRX, and thermally-driven grain growth.

2. Orthogonal Cutting Process Modeling

2.1 Experiments

The orthogonal cutting experiments of AA 1100 investigated in this study were performed by Ni et al. [1] using ceramic cutting tool inserts with a rake angle of -5° at a cutting speed of 0.6 m/s, and a feed of 0.3 mm/rev. Both dry and wet cutting conditions were applied. These orthogonal cutting tests were stopped, and the work material ahead of the tool tip was obtained to evaluate any microstructure change. As shown in Fig. 1, the microstructures at two selected locations were simulated in this study: location A in the primary deformation zone, and location B in the secondary deformation zone.

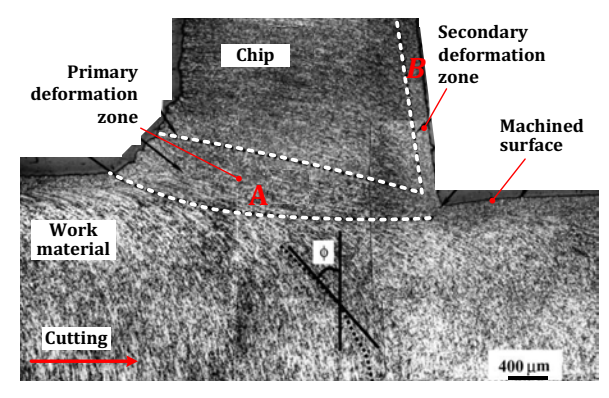


Fig. 1 Optical micrograph of AA 1100 (adapted from [1]).

2.2 FE process model

A 2D FE model was developed using AdvantEdgeTM to evaluate the dynamic thermomechanical loadings at steady state during the cutting process. A 12 mm length of cut was simulated to achieve the steady state status. The Johnson-Cook model of AA 1100 [32] and the silicon nitride-based ceramic tool material was applied in the AdvantEdgeTM model. The coolant heat transfer coefficient was determined as 1500 W/m²-K by a cutting simulation with immersed coolant enabled. The coefficient of friction was determined as 0.5 and 0.3 for the dry

cutting and wet cutting, respectively. Fig. 2 shows the simulated steady-state distributions of temperature and strain rate from the AdvantEdgeTM simulation for the cutting stage. The steady-state cutting temperature distribution simulated by AdvantEdgeTM was then imported into ABAQUS as the initial condition for the cooling stage simulation. An implicit ABAQUS heat transfer analysis was conducted to simulate the cooling temperature history under a natural convection.

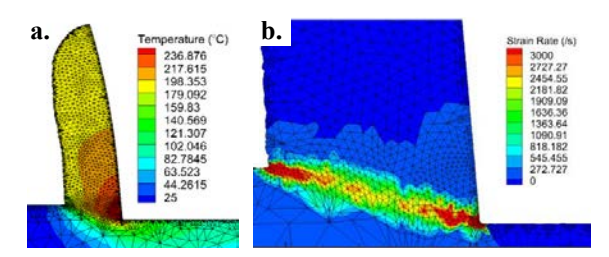


Fig. 2 Steady-state dry cutting simulation using AdvantEdgeTM: (a) temperature; (b) strain rate.

3. Dislocation Density-Based Modeling of DRX and Grain Growth

A new dislocation density-based DRX model is developed in this study considering the dynamic thermomechanical loadings, DRX and grain growth kinetics during the cutting process. The dislocation density evolution is modeled through the approach adapted from the authors' previous work [24–26] for the work material subjected to the dynamic thermomechanical loadings during machining. The initiation of DRX at elevated temperatures is modeled using a criterion of critical dislocation density [13–17]. The dislocation density evolution model is integrated with DRX and grain growth kinetics model adapted from [15].

3.1 Evolution of Dislocation Density

Under severe plastic deformation, the formation of dislocation cell structure is evaluated by the dislocation generation due to plastic deformation, dislocation annihilation by dynamic recovery, and interaction between the dislocation cell interiors and cell walls. The dislocation density evolution rate on the dislocation cell walls and cell interior are given by:

$$\dot{\rho}_c = \alpha^* \frac{1}{\sqrt{3}b} \sqrt{\rho_w} \cdot \dot{\gamma}_w^r - \beta^* \frac{6}{bd(1-f)^{1/3}} \dot{\gamma}_c^r$$

$$-k_o \left(\dot{\gamma}_c^r / \dot{\gamma}_o \right)^{-1/n} \rho_c \cdot \dot{\gamma}_c^r$$
(1)

$$\dot{\rho}_{w} = \beta^{*} \frac{\sqrt{3} (1-f)}{fb} \sqrt{\rho_{w}} \cdot \dot{\gamma}_{c}^{r} + \beta^{*} \frac{6(1-f)^{\frac{2}{3}}}{bdf} \dot{\gamma}_{c}^{r}$$

$$-k_{o} \left(\dot{\gamma}_{w}^{r} / \dot{\gamma}_{o}\right)^{-1/n} \rho_{w} \cdot \dot{\gamma}_{w}^{r}$$
(2)

where $\dot{\rho}_c$ and $\dot{\rho}_w$ are the dislocation density evolution rate in cell interior and cell walls, respectively. Dislocation evolution rate control parameters are denoted as α^* , β^* and k_o . b is the magnitude of Burgers vector, d is the dislocation cell size. $\dot{\gamma}_w^r$ and $\dot{\gamma}_c^r$ are the resolved shear strain rates for the cell walls and interiors, respectively. It is assumed that these resolved shear strain rates are equal across the cell walls and cell interiors, i.e.,

Table 1. Model parameters for microstructure evolution model of AA 1100.

α^*	\boldsymbol{eta}^*	k_o	$\dot{\gamma}_o$	f_o	f_{∞}	M_T	$\widetilde{\gamma}^r$	ρ_{wo} (m ⁻²)	$ ho_{co}$ (m ⁻²)	c_{I}	c_2	c_3
0.061	0.011	6.3-7.8	6000	0.25	0.06	3.06	3.2	1e12	1e11	0.02	0.5 [33]	1e28

Table 2. Material physical properties of AA 1100 [34,35].

E (GPa)	G (GPa)	v	b (nm)	ρ (kg/m ³)	T _m (°C)	α (10 ⁻⁶ /°C)	$k_c(W/m \cdot {}^{\circ}C)$	$c_p(J/kg.^{\circ}C)$	Qact (kJ/mol)	Q_b (kJ/mol)	$\delta D_{ob} (\text{m}^3/\text{s})$
68.9	26	0.33	0.286	2710	660	23.6	222	896	142 [36]	82 [36]	5e-14 [36]

 $\dot{\gamma}_w' = \dot{\gamma}_c' = \dot{\gamma}^r$. The resolved shear strain rate $\dot{\gamma}'$ can be calculated by the von Mises strain rate $\dot{\varepsilon}$ using $\dot{\gamma}' = M_T \dot{\varepsilon}$, where M_T is the Taylor factor. $\dot{\gamma}_o$ is the reference resolved shear strain rate. The volume fraction of the dislocation cell wall are denoted as f, which is given by

$$f = f_{\infty} + (f_o - f_{\infty}) \exp(-\gamma^r / \tilde{\gamma}^r)$$
 (3)

where f_o and f_∞ are the initial and saturation volume fractions of cell walls, respectively. $\tilde{\gamma}'$ is a parameter describing the rate of variation of f with resolved shear strain $\dot{\gamma}'$ and adopted to be 3.2 [37]. The total dislocation density $-(\rho_{tot})$, is calculated from a mixture rule:

$$\rho_{tot} = f \rho_w + (1 - f) \rho_c \tag{4}$$

and then the dislocation cell size is given as:

$$d = K_d / \sqrt{\rho_{tot}} \tag{5}$$

where K_d is a material constant and adopted to be 30 in this study for AA 1100 [24].

3.2 DRX nucleation and grain growth kinetics

DRX is able to occur at elevated temperatures as the total dislocation density passes a threshold. Roberts and Ahlblom [38] modeled the critical dislocation density and assumed the subgrain size as the dislocation mean-free path. In prior CA models for DRX during low-strain or quasi-static hot working processes, the subgrain size was estimated based on the steady-state creep stress [39]. Considering the dynamic thermomechanical loadings during machining, the dislocation mean free path was estimated using the dislocation cell size d in this model. The critical dislocation density ρ_{crit} is given by:

$$\rho_{\rm crit} = \left(\frac{c_1 \Gamma_{\rm m} \dot{\varepsilon}}{3bdM_{gb} \xi^2}\right)^{1/3} \tag{6}$$

where Γ_m is the grain boundary energy, M_{gb} is grain boundary mobility, ξ is the dislocation line energy. These are given by:

$$\Gamma_{\rm m} = \frac{Gb\theta_{\rm m}}{4\pi(1-\nu)} \tag{7}$$

$$M_{gb} = \frac{\delta D_{0b}b}{K_b T} \exp(-\frac{Q_b}{RT}) \tag{8}$$

$$\xi = c_2 G b^2 \tag{9}$$

where G is shear modulus, θ_m is misorientation for a high angle boundary (assumed as 15°), ν is Poisson's ratio, K_b is Boltzmann constant, T is temperature in Kelvin, δ is the grain boundary thickness of the material, D_{ob} is the grain boundary self-diffusion coefficient at 0 K; Q_b is activation energy of grain boundary self-diffusion; R is ideal gas constant. c_I , and c_2 are model parameters.

As dislocation density ρ_{tot} exceeds ρ_{crit} , the nucleus of

dynamic recrystallized grains can be formed on a pre-existing grain boundaries subjected to a probabilistic transformation rule. This transformation rule is determined by the DRX nucleation rate, which is a function of the activation energy for deformation (Q_{act}) [15]:

$$\dot{\mathbf{n}}(\dot{\varepsilon}, T) = c_3 \dot{\varepsilon} \exp\left(-Q_{act}/RT\right) \tag{10}$$

where c_3 is a model parameter. Once this transformation rule is satisfied, the dislocation densities $(\rho_c, \rho_w, \text{ and } \rho_{tot})$ will be reset to a strain-free level at the nucleation sites.

Grain growth at the nucleation sites is usually driven by reduction of the total grain boundary energy. A key gradient of dislocation energy presents due to the heterogeneity of dislocation density near the recrystallized grain. The grain boundary tends to move from the recrystallized grain with a low dislocation density to the adjacent matrix grain with a high dislocation density. For a certain recrystallized grain, the grain growth rate (V) is given by:

$$V = M_{gb}F \tag{11}$$

where F is the growth driving force per unit area of this recrystallized grain, which is given by:

$$F = \xi(\rho_{tot,m} - \rho_{tot,DRX}) - 2\Gamma/r \tag{12}$$

where $\rho_{tot,DRX}$ and $\rho_{tot,m}$ are the total dislocation density of this recrystallized grain and its adjacent matrix grains, respectively. r is the radius of this recrystallized grains. Γ is the grain boundary energy between this recrystallized and its adjacent matrix grains, which is given by:

$$\Gamma = \begin{cases} \Gamma_{\text{m}} \frac{\theta}{\theta_{m}} [1 - \ln(\frac{\theta}{\theta_{m}})] & \text{for } \theta \leq \theta_{m} \\ \Gamma_{\text{m}} & \text{for } \theta \leq \theta_{m} \end{cases}$$
(13)

where θ is the orientation difference between this recrystallized grain and its adjacent matrix grains. All the model parameters are given in Table 1. The material physical properties are given in Table 2.

4. CA Model and Simulations

4.1 CA model

The CA model was developed in MATLAB to predict the microstructure evolution during the machining process. The simulation domain was discretised into an array of equally spaced cells which evolve based on the states of neighbouring cells according to a set of transformation rules. Every lattice cell had six state variables, namely grain orientation, total dislocation density, label of grain boundary, index of recrystallization, label of recrystallized grains, and index of colour. 2D von Neumann's nearest neighbouring rule was used in this model. The initial workpiece material microstructure was firstly generated using a grain growth algorithm. The orientation variable was set using a random integer. The

nucleus were set randomly in the domain and grow until the driving force reached zero.

As the simulation of DRX starts, the total dislocation density (i.e., ρ_{tot}) is constantly updated throughout the whole computation domain at each time step, subjected to the temperature and strain rate histories obtained from the FE simulations. As dislocation density exceeds ρ_{crit} , a probabilistic transformation rule is applied to ensure a random distribution of DRX nucleus. A random number $P(0 \le P \le 1)$ is assigned on the grain boundary cells, and compared with the nucleation probability, P_{nuc} . For P less than P_{nuc} , the cell becomes a DRX nucleus, and all the state variables are updated accordingly. Otherwise, the cell maintains in the original grain without any change of state variables. P_{nuc} is given by:

$$P_{\text{nuc}} = \dot{n} \times \Delta t \times S_{\text{CA}} \tag{14}$$

where Δt is the time increment and S_{CA} is the area of a lattice cell. For square cells in this study, $S_{CA} = L_{CA}^2$, where L_{CA} is a single cell length.

The newly generated DRX nucleus continues to grow, and the grain boundary migrates continuously. Base on the grain growth kinetics described by Eqs. 11-13, the grain boundary migration distance, L_G , is determined by:

$$L_G = V \Delta t \tag{15}$$

and the radius of this recrystallized grains r is given as [40]:

$$r = \sqrt{N_{DRX} \cdot S_{CA} / \pi} \tag{16}$$

where N_{DRX} is the total number of the CA cells held by this recrystallized grain. As the grain growth rate V is reduced to zero, the grain growth stops. The recrystallization progress is captured by the volume fraction of recrystallized grain, X_{RX} :

$$X_{\rm RX} = \frac{N_{\rm RX}}{N_{\rm X} \cdot N_{\rm y}} \tag{17}$$

where N_{RX} is total cell number in recrystallized grains, N_X and N_Y are the total cell number along X- and Y-axis in the 2D simulation domain.

4.2 CA simulations

The formation of recrystallized microstructures in the primary (location A) and secondary (location B) deformation zones shown in Fig. 1 is simulated. Table 3 lists the simulation conditions. The thermomechanical loading histories during both cutting and cooling stage were extracted from the corresponding FE simulations for each location.

Table 3. CA simulations.

Sim.	Location	Coolant	Simulation Domain (µm²)	L _{CA} (nm)
1	A	No	4×2	10
2	В	No	20×10	50
3	В	Yes	4×2	10

A simulation domain of 400×200 square cells was used in this study with the resolution determined by L_{CA} . Two domain sizes were used, $4\times2~\mu\text{m}^2$ and $20\times10~\mu\text{m}^2$, in which L_{CA} was 10 nm and 50 nm, respectively. The CA simulation consisted of two stages corresponding to the cutting and cooling stages. Unlike other CA simulations in literature, the time increment in this model was not constant. A time increment of 15 μ s was applied during the cutting stage; whereas it was 5 ms during the

cooling stage.

4.3 Simulation results and discussion

Fig. 3 shows the simulated microstructures from the CA model and compares the simulation results with the experimental results from [1]. Under the dry cutting condition, different microstructures were simulated in the primary and secondary deformation zones. For the primary deformation zone (location A), Fig. 3a shows small DRX nuclei are formed sporadically along the grain boundary of the pre-existing grains. The process of recrystallization was initiated but did not complete. A bimodal distribution of grain size as shown in Fig. 3h captures both the DRX nuclei and pre-existing sheared grains. The peak near 50 nm corresponds to the small DRX nuclei. In the secondary deformation zone (location B), Fig. 3b shows the process of recrystallization completes and the whole domain were replaced by the recrystallized grains. The simulation results match well with the TEM micrograph as shown in Fig. 3e.

The effect of cutting process temperature is further investigated in by comparing the simulations in the secondary deformation zone under dry and wet cutting conditions. Under the wet cutting condition, an ultrafine grain structure was obtained as can be seen in Fig. 3c, and the whole domain was occupied with submicron recrystallized grains. Under the dry cutting condition, grains are relatively larger (greater than 1 μm) and have undergone a more significant thermally-driven grain growth process, i.e., grain coarsening. These results are mainly caused by the different temperature loadings from the two cutting conditions.

The temperature histories in the secondary deformation zone were simulated as shown in Fig. 4a for the two cutting conditions. During dry cutting, the work material temperature reached to 248 °C $(0.56T_m)$ by the end of cutting process. Then, it maintains a high temperature greater than $0.5T_m$ for additional 2 s during the cooling process. In comparison, under the wet cutting condition, the work material temperature was much lower and never exceeded $0.5T_m$, due to a combining effect of cooling and lubrication of the cutting fluid. It has been extensively reported that the thermally-driven grain growth is more significant when temperature is above $0.5-0.6T_m$ [12]. Under the dry cutting condition, the work material in the secondary deformation zone underwent a more significant grain coarsening after the completion of recrystallization. In addition, the simulated evolutions of volume fraction of the recrystallized grains were significantly different under the two cutting conditions as shown in Fig. 4b. During dry cutting, it took about 0.3 s to complete the recrystallization, whereas it took about 0.6 s under the wet cutting condition.

The simulation results show that DRX is initiated as the work material passes through the primary deformation zone to the chip, and requires an additional time to complete. As material passes to the secondary deformation zone after 1 ms, X_{RX} was only about 3% and 1% for dry and wet cutting conditions, respectively. The recrystallization process continued and eventually formed the final microstructure inside the chip after the cutting process.

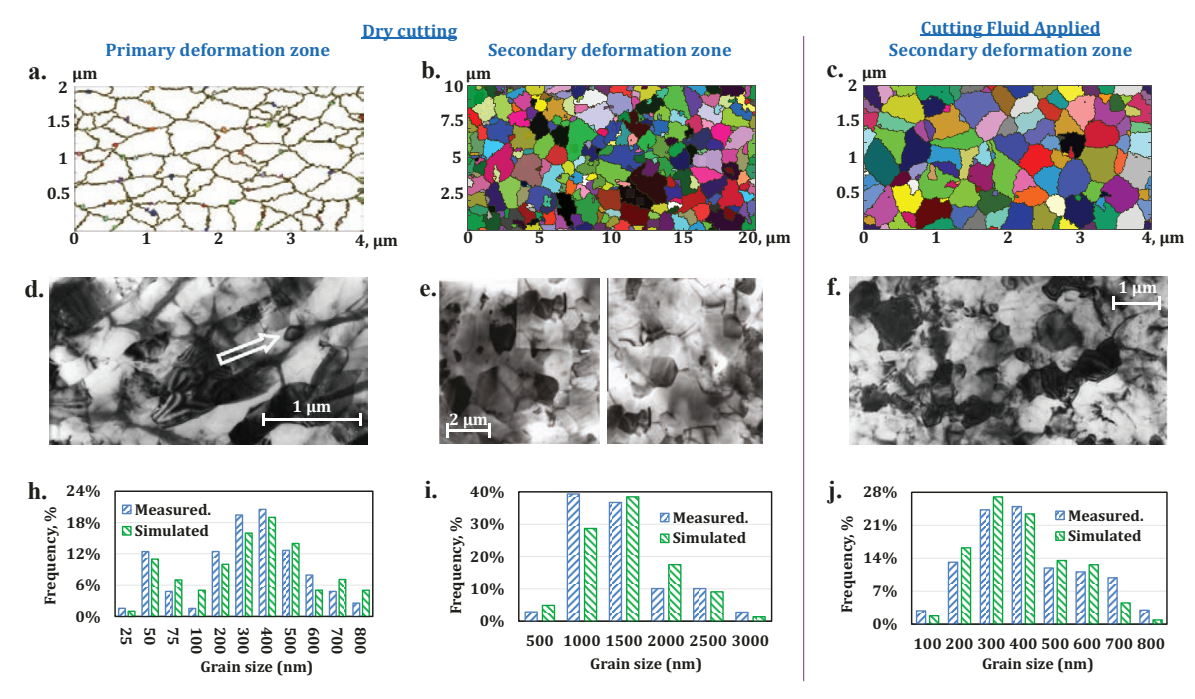


Fig. 3 Simulated microstructures (a-c), TEM micrographs (d-f), and histograms of the measured and predicted grain size distributions (h-j) for three CA simulations (Sim. 1 the bottom of the shear zone in dry cutting, Sim. 2 for the chip surface layer in dry cutting, and Sim. 3 for the chip surface layer with cutting fluid). TEM micrographs are adopted from [1].

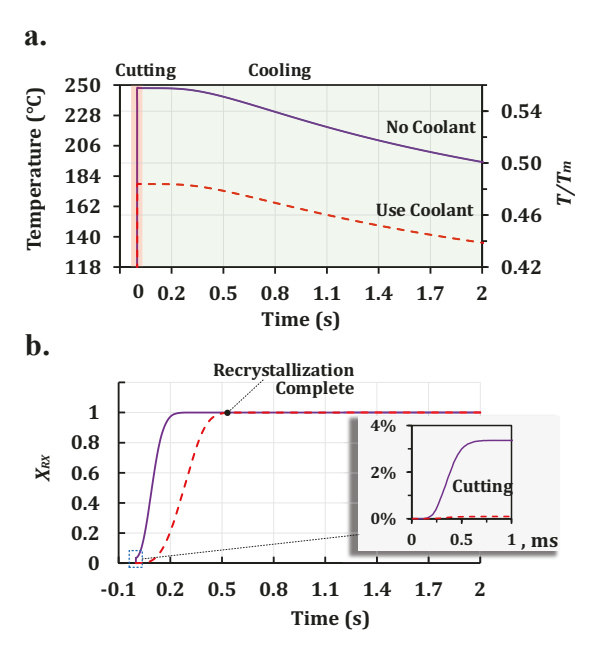


Fig. 4 Effect of coolant on microstructure evolution: (a) temperature history simulated by the FE model in the chip surface layer over both cutting and cooling stages; (b) X_{RX} history simulated by the CA model in the chip surface layer simulated over both cutting and cooling stages.

5. Conclusions

A CA model was successfully developed for the first time to simulate the work material microstructure evolution during orthogonal cutting. The microstructure changes in the primary and secondary deformation zones for AA 1100 under dry or wet cutting conditions were discussed. A new dislocation density-based kinetics model was developed for the machining process. The CA simulation results agreed with the experimental results reported in literature very well. Based on experimental analysis and simulation results, for the fully recrystallized domain (e.g., the secondary deformation zone), temperature was found to be the major factor to determine the microstructure evolution.

Acknowledgements

The authors gratefully acknowledge the financial support by the National Science Foundation under Grant Number CMMI-1537512.

References

- [1] Ni, H., Elmadagli, M., and Alpas, A. T., 2004, "Mechanical properties and microstructures of 1100 aluminum subjected to dry machining," Materials Science and Engineering: A, 385(1–2), pp. 267–278.
- [2] Ni, H., and Alpas, A. T., 2003, "Sub-micrometer structures generated during dry machining of copper," Materials Science and Engineering: A, 361(1–2), pp. 338–349.
- [3] Swaminathan, S., Shankar, M. R., Lee, S., Hwang, J., King, A. H., Kezar, R. F., Rao, B. C., Brown, T. L., Chandrasekar, S., Compton, W. D., and Trumble, K. P., 2005, "Large strain deformation and ultra-fine grained materials by machining," Materials Science and Engineering: A, 410–411, pp. 358–363.

- [4] Shankar, M. R., Chandrasekar, S., King, A. H., and Compton, W. D., 2005, "Microstructure and stability of nanocrystalline aluminum 6061 created by large strain machining," Acta Materialia, 53(18), pp. 4781–4793.
- [5] Elmadagli, M., and Alpas, A. T., 2003, "Metallographic analysis of the deformation microstructure of copper subjected to orthogonal cutting," Materials Science and Engineering: A, 355(1-2), pp. 249– 259
- [6] Sellars, C. M., 1990, "Modelling microstructural development during hot rolling," Materials Science and Technology, 6(11), pp. 1072–1081.
- [7] Yada, H., 1988, "Prediction of Microstructural Changes and Mechanical Properties in Hot Strip Rolling," Proceedings of the Metallurgical Society of the Canadian Institute of Mining and Metallurgy, Elsevier, pp. 105–119.
- [8] Laasraoui, A., and Jonas, J. J., 1991, "Recrystallization of austenite after deformation at high temperatures and strain rates analysis and modeling," Metallurgical transactions. A, Physical metallurgy and materials science, 22 A(1), pp. 151–160.
 [9] Kim, S.-L., and Yoo, Y.-C., 2001, "Dynamic recrystallization
- [9] Kim, S.-I., and Yoo, Y.-C., 2001, "Dynamic recrystallization behavior of AISI 304 stainless steel," Materials Science and Engineering: A, 311(1-2), pp. 108-113.
- [10] Yanagimoto, J., Karhausen, K., Brand, A. J., and Kopp, R., 1998, "Incremental Formulation for the Prediction of Flow Stress and Microstructural Change in Hot Forming," ASME Journal of Manufacturing Science and Engineering, 120(2), p. 316.
- [11] Behnagh, R. A., Shen, N., Ansari, M. A., Narvan, M., Besharati Givi, M. K., and Ding, H., 2015, "Experimental Analysis and Microstructure Modeling of Friction Stir Extrusion of Magnesium Chips," ASME Journal of Manufacturing Science and Engineering, 138(4), p. 41008.
- [12] Shen, N., Samanta, A., Ding, H., and Cai, W. W., 2016, "Simulating microstructure evolution of battery tabs during ultrasonic welding," SME Journal of Manufacturing Processes, 23, pp. 306–314
- pp. 306–314.
 Zheng, C., Xiao, N., Li, D., and Li, Y., 2008, "Microstructure prediction of the austenite recrystallization during multi-pass steel strip hot rolling: A cellular automaton modeling," Computational Materials Science, 44(2), pp. 507–514.
- [14] Kugler, G., and Turk, R., 2004, "Modeling the dynamic recrystallization under multi-stage hot deformation," Acta Materialia, 52(15), pp. 4659–4668.
 [15] Ding, R., and Guo, Z. ., 2001, "Coupled quantitative simulation of
- [15] Ding, R., and Guo, Z. ., 2001, "Coupled quantitative simulation of microstructural evolution and plastic flow during dynamic recrystallization" Acta Materialia 49(16), pp. 3163–3175
- recrystallization," Acta Materialia, **49**(16), pp. 3163–3175.

 [16] Yin, H., and Felicelli, S. D., 2009, "A cellular automaton model for dendrite growth in magnesium alloy AZ91," Modelling and Simulation in Materials Science and Engineering, **17**(7), p. 75011.
- [17] Zhang, Y., Jiang, S., Liang, Y., and Hu, L., 2013, "Simulation of dynamic recrystallization of NiTi shape memory alloy during hot compression deformation based on cellular automaton," Computational Materials Science, 71, pp. 124–134.
- [18] Rotella, G., Dillon, O. W., Umbrello, D., Settineri, L., and Jawahir, I. S., 2013, "Finite element modeling of microstructural changes in turning of AA7075-T651 Alloy," Journal of Manufacturing Processes, 15(1), pp. 87–95.
 [19] Tabei, A., Shih, D. S., Garmestani, H., and Liang, S. Y., 2016,
- [19] Tabei, A., Shih, D. S., Garmestani, H., and Liang, S. Y., 2016, "Dynamic Recrystallization of Al Alloy 7075 in Turning," Journal of Manufacturing Science and Engineering, 138(7), p. 71010.
- [20] Jafarian, F., Imaz Ciaran, M., Umbrello, D., Arrazola, P. J., Filice, L., and Amirabadi, H., 2014, "Finite element simulation of machining Inconel 718 alloy including microstructure changes," International Journal of Mechanical Sciences, 88, pp. 110–121.
- [21] Pu, Z., Umbrello, D., Dillon, O. W., Lu, T., Puleo, D. a., and Jawahir, I. S., 2014, "Finite element modeling of microstructural changes in dry and cryogenic machining of AZ31B magnesium alloy," SME Journal of Manufacturing Processes, 16(2), pp. 335– 343.
- [22] Outeiro, J. C., Rossi, F., Fromentin, G., Poulachon, G., Germain, G., and Batista, A. C., 2013, "Process Mechanics and Surface Integrity Induced by Dry and Cryogenic Machining of AZ31B-O Magnesium Alloy," Procedia CIRP, 8, pp. 487–492.
- Magnesium Alloy," Procedia CIRP, 8, pp. 487–492.

 [23] Umbrello, D., Caruso, S., and Imbrogno, S., 2016, "Finite element modelling of microstructural changes in dry and cryogenic machining AISI 52100 steel," Materials Science and Technology,
- [24] Ding, H., Shen, N., and Shin, Y. C., 2011, "Modeling of grain refinement in aluminum and copper subjected to cutting,"

- Computational Materials Science, 50(10), pp. 3016–3025.

 [25] Shen, N., Ding, H., Pu, Z., Jawahir, I. S., and Jia, T., 2017,
 "Enhanced Surface Integrity from Cryogenic Machining of AZ31B
 Mg Alloy: A Physics-Based Analysis with Microstructure
 Prediction," ASME Journal of Manufacturing Science and
 Engineering 139(6) p. 61012
- Engineering, **139**(6), p. 61012.

 [26] Ding, H., and Shin, Y. C., 2014, "Dislocation Density-Based Grain Refinement Modeling of Orthogonal Cutting of Titanium," ASME Journal of Manufacturing Science and Engineering, **136**(4), p. 41003.
- [27] Liu, R., Salahshoor, M., Melkote, S. N., and Marusich, T., 2014, "A unified internal state variable material model for inclastic deformation and microstructure evolution in SS304," Materials Science and Engineering: A, 594, pp. 352–363.
 [28] Atmani, Z., Haddag, B., Nouari, M., and Zenasni, M., 2016,
- [28] Atmani, Z., Haddag, B., Nouari, M., and Zenasni, M., 2016, "Combined microstructure-based flow stress and grain size evolution models for multi-physics modelling of metal machining," International Journal of Mechanical Sciences, 118, pp. 77–90.
- [29] Liu, R., Salahshoor, M., Melkote, S. N., and Marusich, T., 2014, "The Prediction of Machined Surface Hardness Using a New Physics-based Material Model," Procedia CIRP, 13, pp. 249–256.
- [30] Liu, R., Salahshoor, M., Melkote, S. N., and Marusich, T., 2015, "A unified material model including dislocation drag and its application to simulation of orthogonal cutting of OFHC Copper," Journal of Materials Processing Technology, 216, pp. 328–338.
 [31] Ding, L., Zhang, X., and Richard Liu, C., 2014, "Dislocation
- [31] Ding, L., Zhang, X., and Richard Liu, C., 2014, "Dislocation Density and Grain Size Evolution in the Machining of Al6061-T6 Alloys," Journal of Manufacturing Science and Engineering, 136(4), p. 41020.
- 136(4), p. 41020.
 [32] Asghar, S. A., Mousavi, A., and Bahador, S. R., 2011, "Investigation and numerical analysis of strain distribution in the twist extrusion of pure aluminum," JOM, 63(2), pp. 69–76.
- [33] Huang, Y., and Humphreys, F. J., 1997, "Transient dynamic recrystallization in an aluminium alloy subjected to large reductions in strain rate," Acta Materialia, 45(11), pp. 4491–4503.
- [34] Davis, J. R., 1990, Properties and selection: nonferrous alloys and special-purpose materials, ASM International.
- [35] Holt, J. M., Mindlin, H., Ho, C. Y., University., P., and Synthesis., C. for I. and N. D. A. and, 1997, Structural alloys handbook, CINDAS/Purdue University. West Lafavette. Ind.
- CINDAS/Purdue University, West Lafayette, Ind.

 Frost, H. J., and Ashby, F., 1982, Deformation-mechanism maps: the plasticity and creep of metals and ceramics, Pergamon Press, Kidlington, Oxford, United Kingdom.
- Baik, S. C., Estrin, Y., Kim, H. S., and Hellmig, R. J., 2003, "Dislocation density-based modeling of deformation behavior of aluminium under equal channel angular pressing," Materials Science and Engineering A, 351, pp. 86–97.
 Roberts, W., and Ahlblom, B., 1978, "A nucleation criterion for
- [38] Roberts, W., and Ahlblom, B., 1978, "A nucleation criterion for dynamic recrystallization during hot working," Acta Metallurgica, 26, pp. 801–813.
- [39] Takeuchi, S., and Argon, A. S., 1976, "Steady-state creep of single-phase crystalline matter at high temperature," Journal of Materials Science, 11(8), pp. 1542–1566.
- [40] Chen, F., Qi, K., Cui, Z., and Lai, X., 2014, "Modeling the dynamic recrystallization in austenitic stainless steel using cellular automaton method," Computational Materials Science, 83, pp. 331–